Supplement of

Cryogenic Fractionation and Thaw-Gradient Reorganization of Carbon, Nutrient and Trace Element Pools in Permafrost Peatlands

Lucia Pérez-Serrano et al.

Correspondence to: Lucia Pérez-Serrano (lucia.perez-serrano@utoulouse.fr)

Table S1. Radiocarbon (^{14}C) dates from peat cores at Tz-1(n = 3), Tz-2 (n = 6), Tz-3 (n = 5), and Tz-4 (n = 7).

Core	Depth (cm)	Material dated	Lab number	$F^{14}C \pm SD$	Calibrated ranges at 95.4% (cal. BP)	Median (cal. BP)
Tz-4	5	peat	GifA24280, ECHo-6312	0.7102 ± 0.0019	2981–2907 (1.8 %), 2881–2775(93.7%)	2823
Tz-4	15	peat	GifA24281, ECHo-6313	0.6449 ± 0.0018	3881–3811 (33.3 %), 3805–3715 (61.6 %), 3706–3702 (0.5 %)	3782
Tz-4	25	peat	GifA24282, ECHo-6314	0.5321 ± 0.0016	5902–5745	5816
Tz-4	50	peat	GifA24283, ECHo-6315	0.4502 ± 0.0014	7423–7377 (36.9 %), 7364–7269 (58.6%)	7340
Tz-4	100	peat	GifA24284, ECHo-6316	0.4239 ± 0.0013	7787–7671	7718
Tz-4	150	peat	GifA24285, ECHo-6317	0.4038 ± 0.0013	8171–8024	8106
Tz-4	180	peat	GifA24286, ECHo-6318	0.3888 ± 0.0013	8422–8359	8391
Tz-3	10	peat	GifA24275, ECHo-6307	0.9631 ± 0.0025	445–355 (72.1 %), 334–301 (23.4 %)	393
Tz-3	30	peat	GifA24276, ECHo-6308	0.7976 ± 0.0021	1785–1763 (3.3 %), 1749–1694 (71.0 %), 1667–1624 (21.2 %)	1716
Tz-3	50	peat	GifA24277, ECHo-6309	0.7300 ± 0.0019	2763–2695 (30.7 %), 2639–2613 (17.5 %), 2594–2499 (47.3 %)	2617
Tz-3	100	peat	GifA24278, ECHo-6310	0.6356 ± 0.0017	4080–4037 (13.3 %), 3995–3885 (81.7 %)	3950
Tz-3	150	peat	GifA24279, ECHo-6311	0.5439 ± 0.0016	5659–5585	5625
Tz-2	10	peat	SacA74631	0.9766 ± 0.0028	294–258 (21.2 %), 224–141 (57.1 %), 31–0 (17.1 %)	190
Tz-2	50	peat	SacA74632	0.8381 ± 0.0025	1350–1294	1323
Tz-2	85	peat	SacA74633	0.8085 ± 0.0025	1697–1663 (26.3 %), 1627–1539 (71.9 %)	1597
Tz-2	110	peat	SacA74634	0.6791 ± 0.0023	3389–3240	3330
Tz-2	140	peat	SacA74635	0.4579 ± 0.0019	7271–7156 (88.5 %), 7115–7069 (5.4 %), 7045–7027 (1.6%)	7210
Tz-2	180	peat	SacA74636	0.4184 ± 0.0019	7935–7739	7843
Tz-1	10	peat	SacA74627	1.2667 ± 0.0031	-	-
Tz-1	50	peat	SacA74628	0.7120 ± 0.0024	2871–2763	2815
Tz-1	75	peat	SacA74629	0.6623 ± 0.0025	3263–3603 (2.9 %), 3588–3454 (92.6 %)	3526
Tz-1	130	peat	SacA74630	0.6144 ± 0.0022	4422–4246	4354

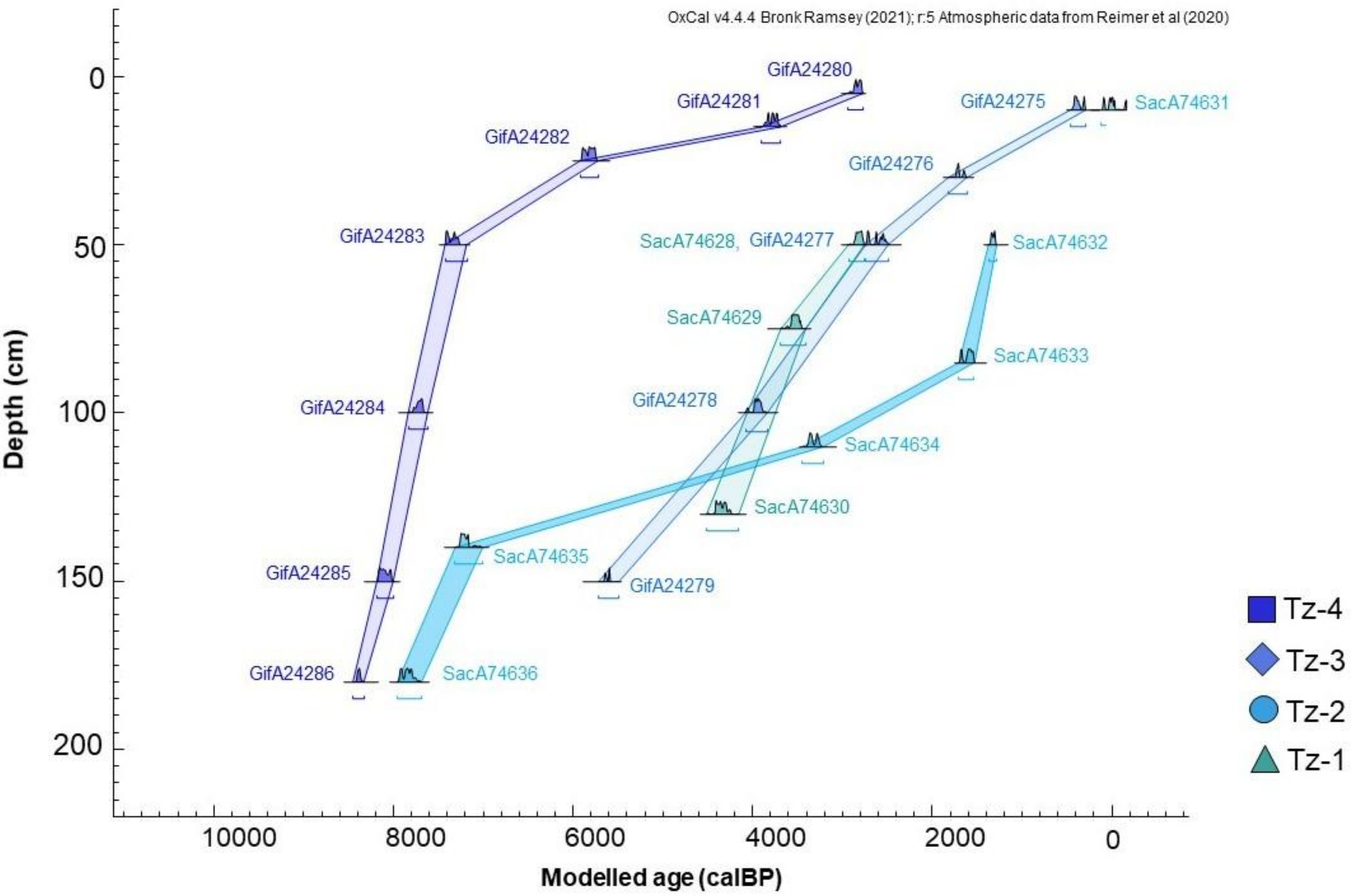

Figure S1. Age-depth models based on C^{14} for Tz-4, Tz-3, Tz-2 and Tz-1 versus depth. Colored areas provide the 95.4 % confidence ranges of the model. Sample SacA74627 is omitted from the model since the corresponding $F^{14}C$ (> 1) might be post-1950.

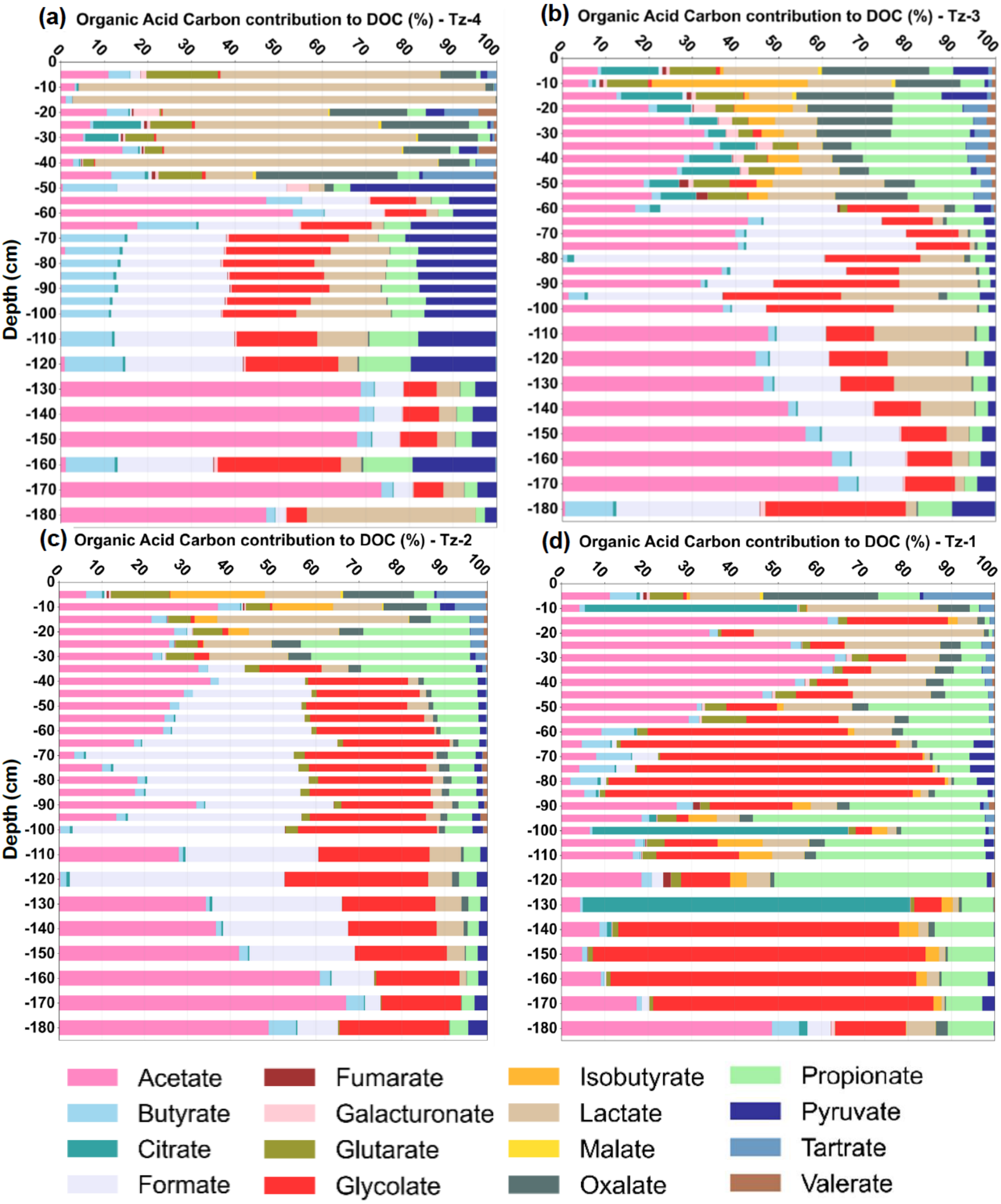

Figure S2. Percentage contribution from organic acids Carbon to the dissolved organic carbon (DOC) pool (< 0.45 µm) for (a) Tz-4, (b) Tz-3, (c) Tz-2 and (d) Tz-1. Horizon thickness corresponds to ± 5 cm up to 100 cm, and ± 10 cm for horizons deeper than 100 cm.

For Tz-4 (bog, Figure S1a), a marked shift occurs between the active layer—dominated by lactate, oxalate, glutarate and acetate down to 45 cm—and the frozen layer. In frozen horizons (70–120 cm and 160 cm), a similar distribution of butyrate, formate, glycolate, pyruvate, lactate and propionate are observed, while deeper layers (130–150 cm and 170 cm) show increasing acetate contributions (> 60 %). Tz-3 (trough, Figure S1b) exhibits two contrasting patterns: in the active layer (0–60 cm), oxalate, propionate and citrate are present, whereas these compounds disappear in the frozen layer (60–180 cm), which is dominated by a more uniform distribution of acetate, formate, glycolate and lactate. For Tz-2 (peat transitional fen, Figure S1c), lactate represents 15–45 % between 5 and 30 cm in the active layer, whereas acetate accounts for 21–37% across most depths. Formate appears below 35 cm. In the frozen layer of Tz-2, the distribution becomes more homogeneous, characterized by acetate (0–35%, increasing with depth), formate (30–50 %), glycolate (~30 %), and minimal lactate (< 10 %) in most horizons. At the active layer of Tz-1 (peat-mineral fen), acetate represents 30–60 % of the organic acid C pool (Figure S1d). Glycolate dominates at 55–80 cm and 140–170 cm, whereas acetate constitutes ~50 % at 180 cm. Citrate peaks at 10 cm (59 %) in the active layer and is also prominent at 100 and 130 cm (75 %) in the frozen layer.

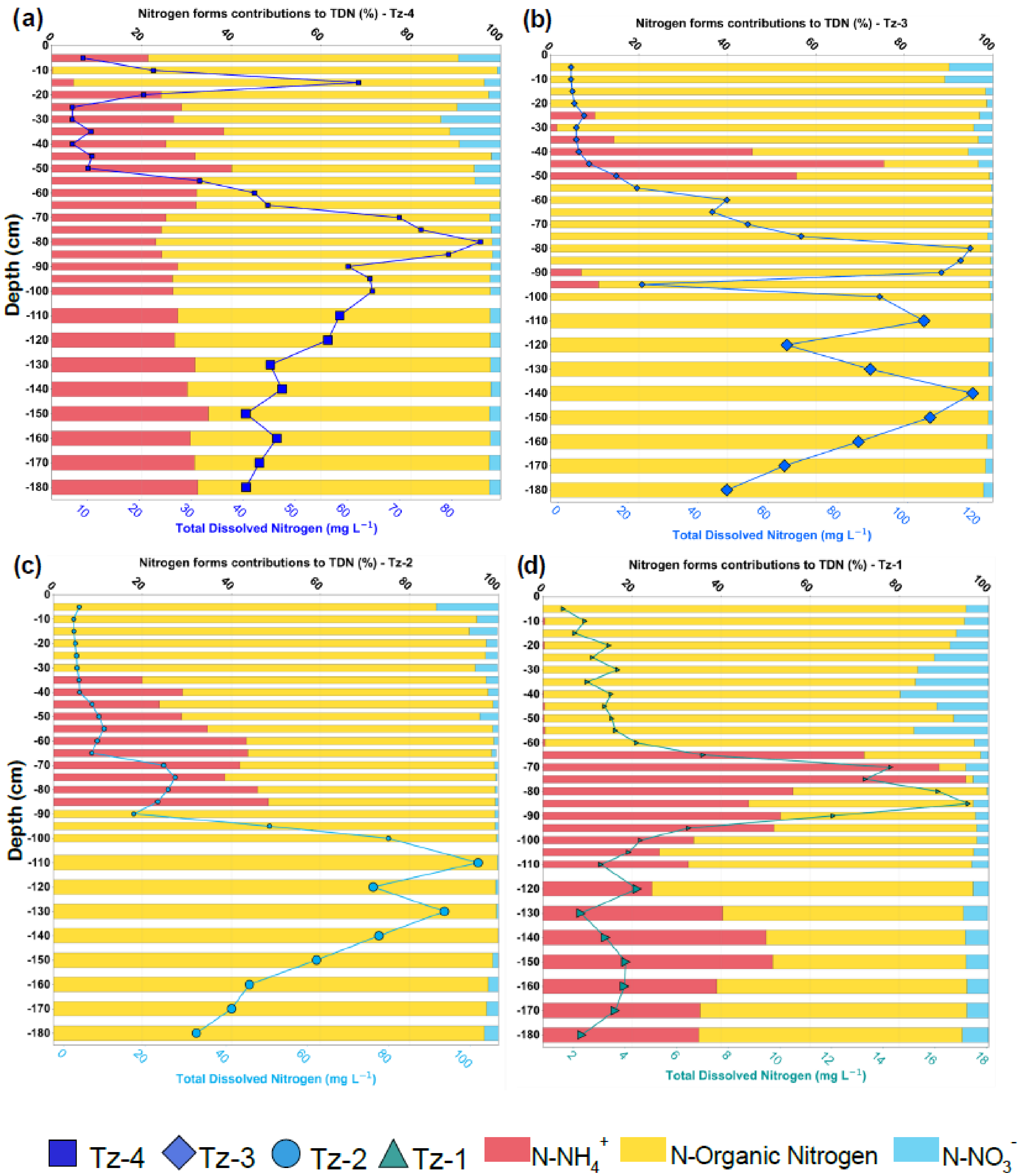

Figure S3. Relative abundance of N forms ($N\text{-}NH_4^+$, N-Organic Nitrogen and $N\text{-}NO_3^-$) in the dissolved Total Nitrogen (TDN) pool (<0.45 µm) for (a) Tz-4, (b) Tz-3, (c) Tz-2 and (d) Tz-1. TDN concentrations (mg L-1) are also represented. Horizon thickness corresponds to ± 5 cm up to 100 cm, and ± 10 cm for horizons deeper than 100 cm.

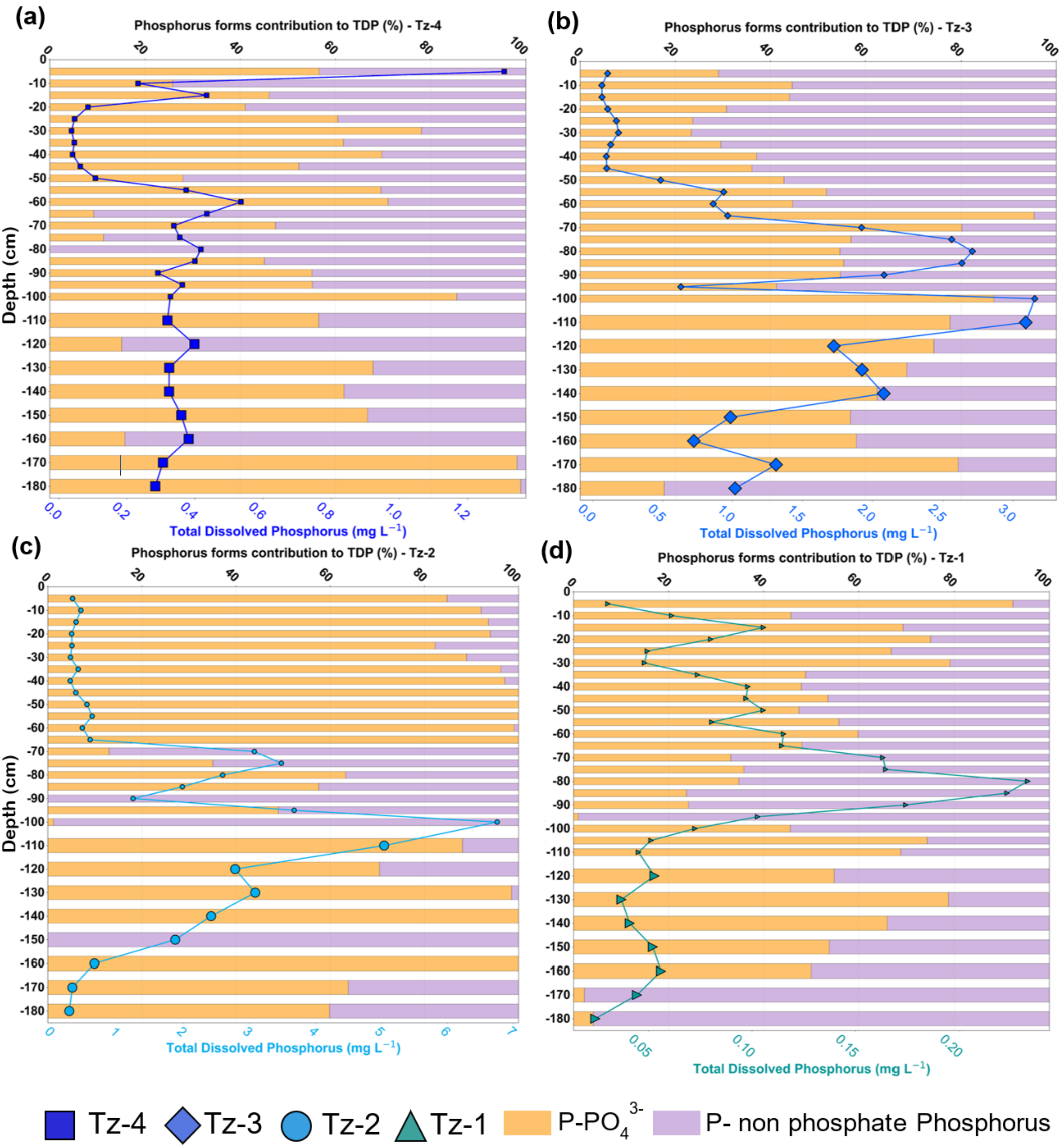

Figure S4. Relative abundance of P forms (phosphate and non-phosphate Phosphorus) in the dissolved Total Phosphorus (TDP) pool (<0.45 µm) for (a) Tz-4, (b) Tz-3, (c) Tz-2 and (d) Tz-1. TDP concentrations (mg L-1) are also represented. Horizon thickness corresponds to ± 5 cm up to 100 cm, and ± 10-cm for horizons deeper than 100 cm. Horizon thickness corresponds to ± 5 cm up to 100 cm, and ± 10 cm for horizons deeper than 100 cm.

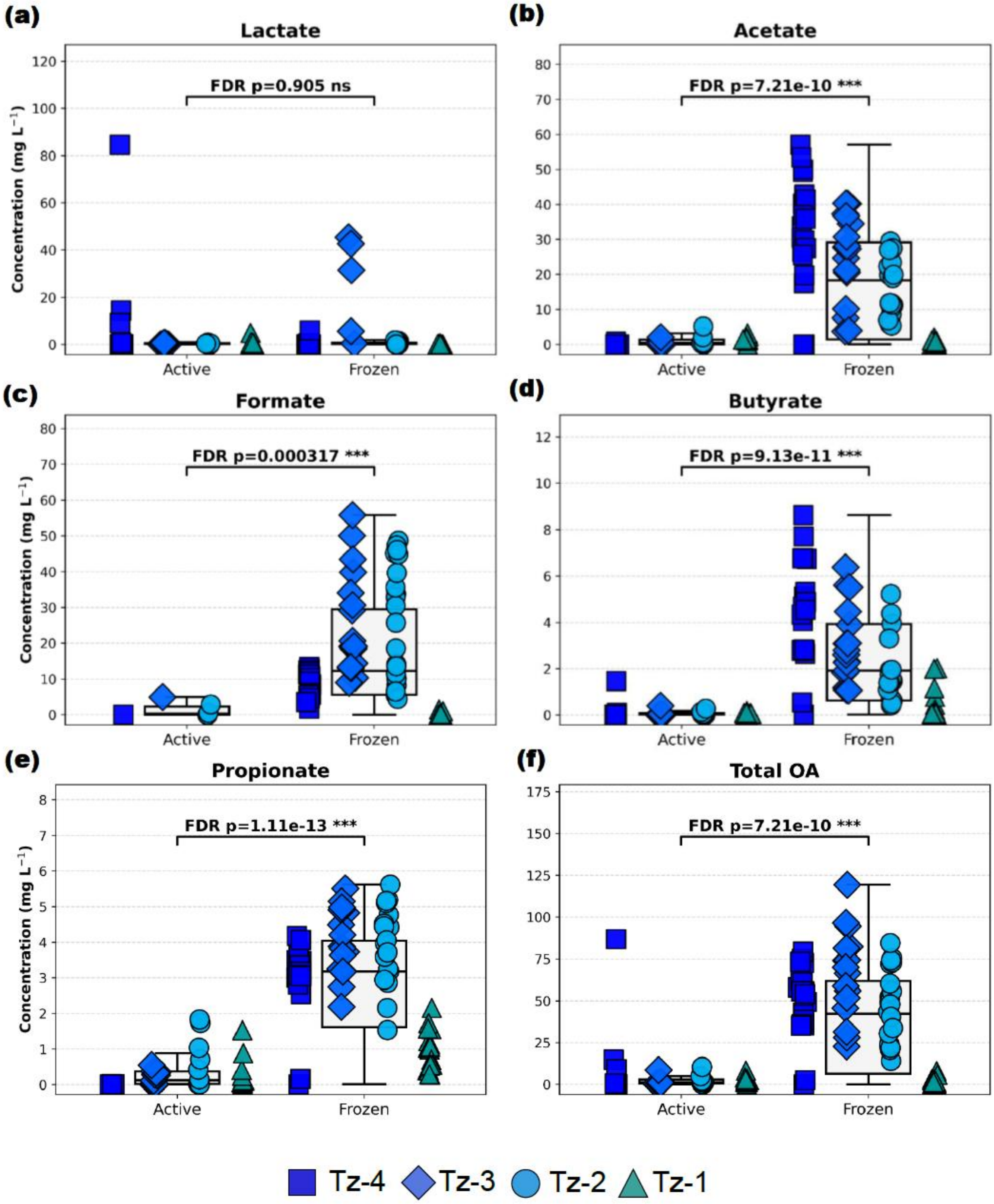

Figure S5. Whisker plots of organic acids concentration (mgC L^{-1}) and p-values (*** $p < 0.001$) in the dissolved phase (< 0.45 µm) for porewater (active layers) and pore ice (frozen layers). The active layers thickness comprises the active layers depth measured at the moment of sampling (40 cm for Tz-4, 60 cm for Tz-3, 40 cm for Tz-2 and 55 cm for Tz-1). Permanent frozen layers are situated between 65 and 180 cm depth.

Table S2. Median concentrations of C from Organic Acids (mg L^{-1}), $SUVA_{254}$ (L mg^{-1} m^{-1}), Fluorescence Index (FI) and DOC (mg L^{-1}) for each layer at each site along with Mann-Whitney U significance test and Kruskal-Wallis test all active and frozen layers comprised (*** p<0.001, ** p<0.01, * p<0.05, ns=not significant).

	Layer and/or site	**$SUVA_{254}$ (L mg^{-1} m^{-1})**	**C from OA (mg L^{-1})**	**Fluorescence Index (FI)**	**DOC (mg L^{-1})**
Median	Tz-4 Active	1.9	0.73	1.03	178.57
	Tz-4 Frozen	0.43	55.48	1.52	306.23
	Tz-3 Active	1.4	1.38	1.08	316.21
	Tz-3 Frozen	0.28	133.73	1.51	742.59
	Tz-2 Active	1.29	1.84	1.17	211.87
	Tz-2 Frozen	0.52	78.32	1.3	579.91
	Tz-1 Active	1.5	2.66	1.27	197.79
	Tz-1 Frozen	0.8	3.82	1.53	171.71
Mann-Whitney U	Tz-4	p = 0.0000 (***)	p = 0.0047 (**)	p = 0.0000 (***)	p = 0.0081 (**)
	Tz-3	p = 0.0001 (***)	p = 0.0000 (***)	p = 0.0000 (***)	p = 0.0001 (***)
	Tz-2	p = 0.0000 (***)	p = 0.0000 (***)	p = 0.0006 (***)	p = 0.0000 (***)
	Tz-1	p =0.0002 (***)	p = 0.1849 (ns)	p = 0.0000 (***)	p = 0.7024 (ns)
Kruskal-Wallis	Active layers	H = 6.44, p = 0.0920 (ns)	H = 4.66, p = 0.1986 (ns)	H = 19.62, p = 0.0002 (***)	H = 16.53, p = 0.0009 (***)
	Frozen layers	H = 12.29, p = 0.0064 (**)	H = 44.55, p = 0.0000 (***)	H = 33.59, p = 0.0000 (***)	H = 49.37, p = 0.0000 (***)

Table S3. Median molar ratios values of C:N, N:P and C:P for each layer at each site along with Mann-Whitney U significance test and Kruskal-Wallis test all active and frozen layers comprised (*** p<0.001, ** p<0.01, * p<0.05, ns=not significant).

	Layer and/or site	C:N	N:P	C:P
Median	Tz-4 Active	20	365	7206
	Tz-4 Frozen	7	320	2439
	Tz-3 Active	52	98	5454
	Tz-3 Frozen	10	99	1016
	Tz-2 Active	72	22	1754
	Tz-2 Frozen	22	38	856
	Tz-1 Active	69	88	6387
	Tz-1 Frozen	28	164	3901
Mann-Whitney U	Tz-4	p = 0.0057 (**)	p = 0.6358 (ns)	p = 0.0792 (ns)
	Tz-3	p = 0.0000 (***)	p = 0.8345 (ns)	p = 0.0000 (***)
	Tz-2	p = 0.0000 (***)	p = 0.0026 (**)	p = 0.1226 (ns)
	Tz-1	p = 0.0003 (***)	p = 0.0001 (***)	p = 0.1849 (ns)
Kruskal-Wallis	Active layers	H = 20.58, p = 0.0001 (***)	H = 22.54, p = 0.0001 (***)	H = 12.31, p = 0.0064 (**)
	Frozen layers	H = 50.19, p = 0.0000 (***)	H = 51.16, p = 0.0000 (***)	H = 45.94, p = 0.0000 (***)

Note on the mass balance projections of C, N and P consumption and export under active layer deepening calculations

The consumption and export model integrates three co-limiting controls on dissolved organic matter consumption: elemental stoichiometry (CNP), substrate kinetics (ICBM), and carbon use efficiency (CUE) after Byun et al. (2025), as a fraction of C consumed by microorganisms can be lost from the system in form of respiration instead of biomass assimilation. Unconsumed dissolved fractions (< 0.45 µm) were assumed to migrate downward the soil column until the hydrological conductivity allows the removal from the soil system. Since deep peat shows a low mineralization potential upon thawing (Estop-Aragonés et al., 2022), and the main focus of this study was to assess the pore ice as a nutrient pool, no priming effect of pore ice on surrounding peat was calculated.

For each depth horizon, dissolved element pools for DOC, TDN and TDP are calculated from dissolved concentrations (mg L^{-1}), water content (%), bulk density (g cm^{-3}) and horizon thickness (cm) using Equation 1:

Eq.1 $$\text{DOC pool (mg m}^{-2}) = \text{Water content (\%)} \times \text{Bulk density (g cm}^{-3}) \times \text{Thickness (cm)} \times \text{DOC (mg L}^{-1}) \times 10$$

Consumption ratios (C:N, C:P) are determined by Eq.2 using the biomass CNP ratios corrected by CUE values (Byun et al., 2025).

Eq.2 $$\text{C:N}_{\text{consumption}} = \frac{\text{C:N}_{\text{biomass}}}{\text{CUE}}$$

If N is non-limiting, then CUE = 0.26, otherwise both N and P are limiting so CUE = 0.49. CUE values vary by site and depth (Table S4); Tz-3 and Tz-1 exhibit lower CUE (0.26), implying higher respiration fractions of consumed C compared to Tz-4 and Tz-2.

Availability of N and P fractions is determined by f_N and f_P limitations (e.g., f_N = (1, C_{cap_N} / C_{total})), and NP co-limitation can be identified in the calculations by stoichiometric sufficiency (f_N, f_P < 1, Table S4) applying a mechanistic multi-substrate co-limitation model (Tang & Riley, 2021) calculated after Equation 2:

Eq.3 $$\lim_{\text{ADD}} = \frac{1}{\frac{1}{f\_N} + \frac{1}{f\_P} - 1} \in [0, 1]$$

DOC pool decomposition was differentiated by ICBM decay rates, separating DOC pool from organic acids (k = 192.7 yr^{-1}, after an average value for acetate and butyrate *k* values), and the rest of the DOC pool (k = 33.7 yr^{-1}) (Drake et al., 2015). The final amount of C that microbial stoichiometric demand allows to be consumed is constrained either by the $\lim_{ADD}$ or the decay rates for DOC pools. Constraint in this model is controlled by CNP stoichiometry, precisely by P scarcity limiting microbiological consumption, contrary to ICBM decay since *k* values allow the degradation of C pools.

The potential export is the dissolved mass that leaves the soil column laterally rather than being consumed or staying as carryover for the next horizon. In Equation 4, horizontal flow is controlled by peat anisotropy determined by bulk density (Beckwith et al., 2003), as in BD < 0.1 g cm^{-3}, $r_{anisotropy}$ = 3; 0.1- 0.2 g cm^{-3}, $r_{anisotropy}$ = 2 ; and 0.2 g cm^{-3}, $r_{anisotropy}$ = 1. L is the distance to the outlet (Fig.S6, Tz-4 = 252.6 m, Tz-3 = 224.6 m, Tz-2 = 89.2 m, Tz-1 = 0 m). The hydraulic gradient (*i*, 0.01188 m s^{-1}) was calculated after the downslope from Tz-4 and Tz-1, and the corresponding water table elevation (Fig. S6).

Eq.4 $$\lambda = \frac{r_{\text{anisotropy}}}{\text{L}} \times \text{i} \left(\frac{\text{m}}{\text{m}}\right) \times \text{thickness (cm)}$$

The carryover fraction is the dissolved pool that is not exported laterally (1- λ) but instead moves vertically downward to the next deeper horizon, represented as the total pool (mg m^{-2}) in Table S4.

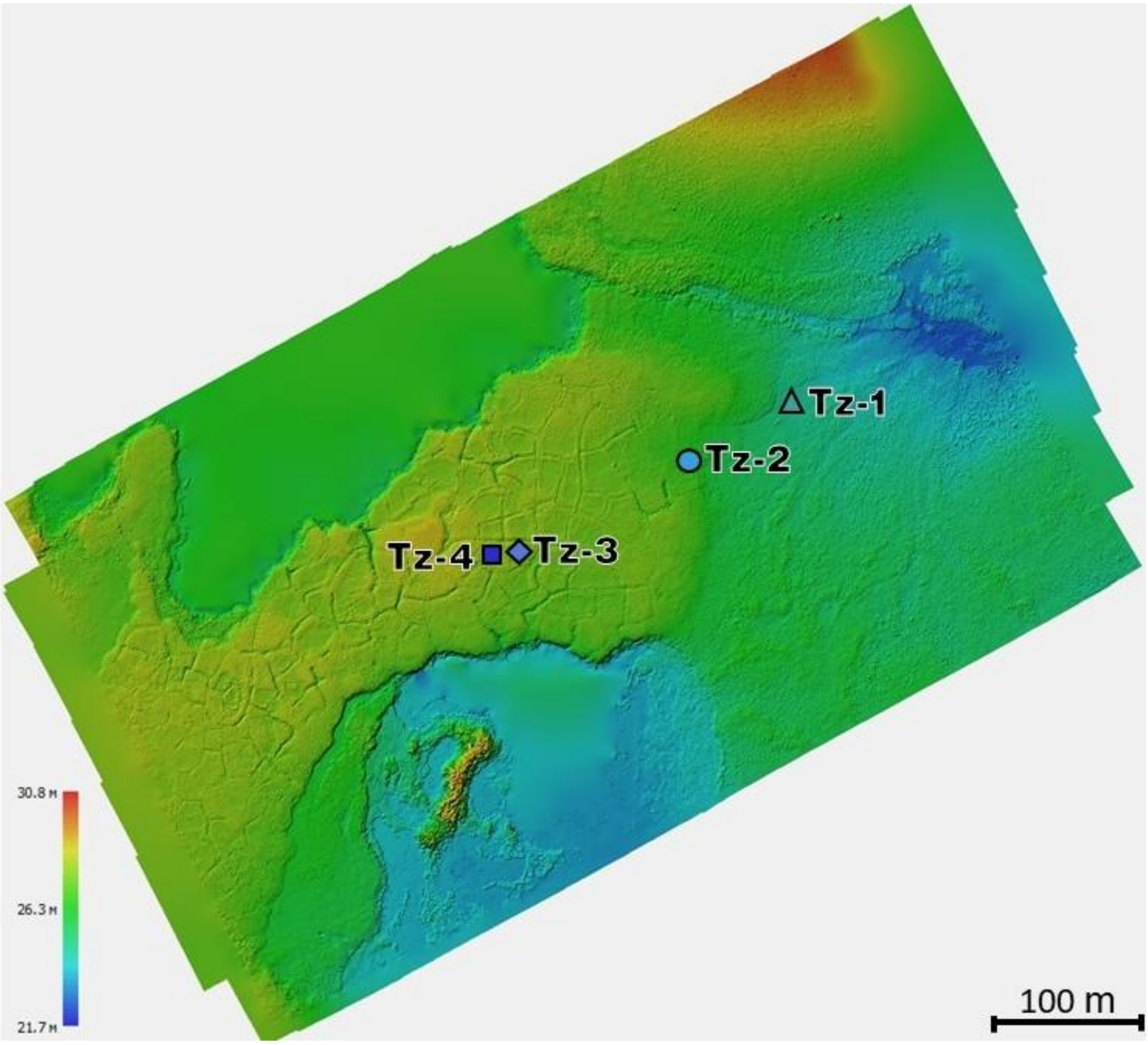

Figure S6. Digital Elevation Model for Tazovsky polygonal peatland.

Table S4. DOC, TDN and TDP pools (mg m^{-2}) along with the consumed pool (%) per horizon in the frozen layer for each core. CUE values were determined for each horizon, as well as N and P co-limitations (f_N, f_P).

			Total pool (mg m^{-2})			Consumed pool (%)					
Site	**Depth interval (cm)**	**Bulk density (g cm^{-3})**	**DOC**	**TDN**	**TDP**	**DOC**	**TDN**	**TDP**	**CUE**	**f_N**	**f_P**
Tz-4	40-45	0.19	13528	505	3	0.46	0.87	99.59	0.49	0.53	0.00
Tz-4	45-50	0.13	18440	1027	6	0.65	0.82	99.83	0.49	0.79	0.01
Tz-4	50-55	0.12	38099	2773	21	2.18	1.12	100	0.26	1.00	0.02
Tz-4	55-60	0.12	54862	5043	29	2.13	0.87	100	0.26	1.00	0.02
Tz-4	60-65	0.09	64836	7166	21	1.30	0.44	100	0.26	1.00	0.01
Tz-4	65-70	0.11	86140	9841	13	0.61	0.20	100	0.26	1.00	0.01
Tz-4	70-75	0.14	106556	13551	18	0.67	0.20	100	0.26	1.00	0.01
Tz-4	75-80	0.14	133452	18438	24	0.72	0.19	100	0.26	1.00	0.01
Tz-4	80-85	0.11	155760	22909	23	0.58	0.15	100	0.26	1.00	0.01
Tz-4	85-90	0.11	170741	26168	16	0.37	0.09	100	0.26	1.00	0.00
Tz-4	90-95	0.13	184805	29186	17	0.37	0.09	100	0.26	1.00	0.00
Tz-4	95-100	0.10	198663	32331	16	0.32	0.07	100	0.26	1.00	0.00
Tz-4	100-110	0.15	248579	39597	40	0.64	0.15	100	0.26	1.00	0.01
Tz-4	110-120	0.12	288871	45835	45	0.62	0.15	100	0.26	1.00	0.01
Tz-4	120-130	0.11	315711	49852	29	0.37	0.09	100	0.26	1.00	0.00
Tz-4	130-140	0.10	348003	55458	39	0.44	0.10	100	0.26	1.00	0.00
Tz-3	60-65	0.15	16775	2067	45	10.79	3.28	100	0.26	1.00	0.11
Tz-3	65-70	0.09	50583	4664	94	7.47	3.04	100	0.26	1.00	0.07
Tz-3	70-75	0.12	93522	8795	157	6.74	2.69	100	0.26	1.00	0.07
Tz-3	75-80	0.09	139028	14041	126	3.63	1.35	100	0.26	1.00	0.04
Tz-3	80-85	0.09	185506	19837	137	2.96	1.04	100	0.26	1.00	0.03
Tz-3	85-90	0.10	236071	25553	113	1.91	0.66	100	0.26	1.00	0.02
Tz-3	90-95	0.05	250850	26910	40	0.64	0.22	100	0.26	1.00	0.01
Tz-3	95-100	0.11	288201	31406	156	2.17	0.75	100	0.26	1.00	0.02
Tz-3	100-110	0.12	374345	42501	335	3.58	1.18	100	0.26	1.00	0.04
Tz-3	110-120	0.16	427814	50470	223	2.09	0.66	100	0.26	1.00	0.02
Tz-3	120-130	0.15	492691	59329	198	1.61	0.50	100	0.26	1.00	0.02
Tz-3	130-140	0.15	561950	69393	182	1.30	0.39	100	0.26	1.00	0.01
Tz-3	140-150	0.19	641171	80577	106	0.66	0.20	100	0.26	1.00	0.01
Tz-3	150-160	0.18	706153	89151	74	0.42	0.12	100	0.26	1.00	0.00
Tz-2	40-45	0.05	10354	172	9	1.72	3.82	97.91	0.49	0.45	0.02
Tz-2	45-50	0.09	25312	497	21	1.63	3.06	98.57	0.49	0.53	0.02
Tz-2	50-55	0.12	43263	947	29	1.34	2.26	99.08	0.49	0.59	0.01
Tz-2	55-60	0.12	58881	1332	23	0.79	1.28	99.50	0.49	0.61	0.01
Tz-2	60-65	0.05	73089	1690	32	0.88	1.40	99.48	0.49	0.63	0.01
Tz-2	65-70	0.08	104190	2921	157	3.01	3.97	99.05	0.49	0.76	0.03
Tz-2	70-75	0.07	142739	4512	218	3.08	3.59	99.49	0.49	0.86	0.03
Tz-2	75-80	0.08	169746	5654	133	1.58	1.75	99.83	0.49	0.90	0.02
Tz-2	80-85	0.07	195111	6756	103	1.07	1.14	99.93	0.49	0.94	0.01
Tz-2	85-90	0.06	214569	7636	68	0.65	0.67	99.98	0.49	0.96	0.01
Tz-2	90-95	0.09	248913	10151	186	2.85	1.37	100	0.26	1.00	0.03
Tz-2	95-100	0.07	298084	13821	322	4.11	1.74	100	0.26	1.00	0.04
Tz-2	100-110	0.19	380602	23330	482	4.82	1.54	100	0.26	1.00	0.05
Tz-2	110-120	0.14	418067	28359	197	1.79	0.52	100	0.26	1.00	0.02
Tz-2	120-130	0.19	519673	38456	337	2.47	0.65	100	0.26	1.00	0.02
Tz-2	130-140	0.16	597430	46742	266	1.70	0.42	100	0.26	1.00	0.02
Tz-1	55-60	0.35	4137	157	4	3.75	1.93	100	0.26	1.00	0.04
Tz-1	60-65	0.48	4751	219	4	2.87	1.22	100	0.26	1.00	0.03
Tz-1	65-70	0.47	7866	451	5	2.49	0.85	100	0.26	1.00	0.02
Tz-1	70-75	0.43	6106	434	5	3.35	0.92	100	0.26	1.00	0.03
Tz-1	75-80	0.59	8746	496	7	3.12	1.08	100	0.26	1.00	0.03
Tz-1	80-85	0.85	8828	458	6	2.55	0.96	100	0.26	1.00	0.03
Tz-1	85-90	0.60	7324	369	5	2.77	1.08	100	0.26	1.00	0.03
Tz-1	90-95	0.60	3481	197	3	3.43	1.18	100	0.26	1.00	0.03
Tz-1	95-100	0.33	2948	165	3	3.35	1.17	100	0.26	1.00	0.03
Tz-1	100-110	0.65	9039	211	3	0.63	0.99	99.64	0.49	0.63	0.01
Tz-1	110-120	1.01	15664	231	3	0.35	0.88	99.47	0.49	0.40	0.00
Tz-1	120-130	0.47	3099	144	2	2.84	1.20	100	0.26	1.00	0.03
Tz-1	130-140	0.67	5586	187	2	0.85	0.94	99.91	0.49	0.91	0.01
Tz-1	140-150	0.64	6946	238	3	0.89	0.96	99.93	0.49	0.93	0.01
Tz-1	150-155	0.87	11486	214	3	0.53	1.04	99.48	0.49	0.50	0.01

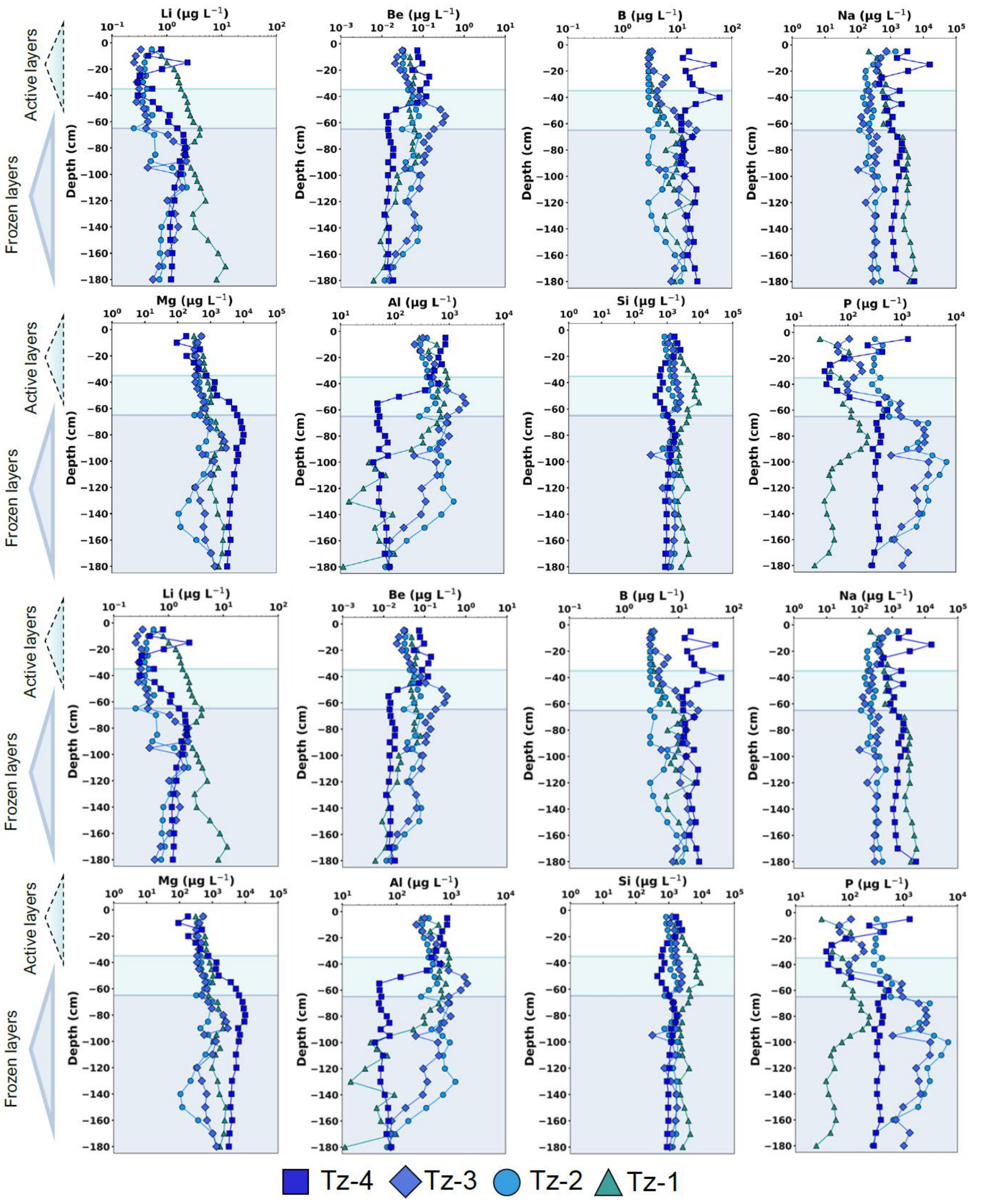
Li (μg L−1)
Be (μg L−1)
B (μg L−1)
Na (μg L−1)
Mg (μg L−1)
Al (μg L−1)
Si (μg L−1)
P (μg L−1)
Depth (cm)
Active layers
Frozen layers
Tz-4
Tz-3
Tz-2
Tz-1

(continuation Figure S7)

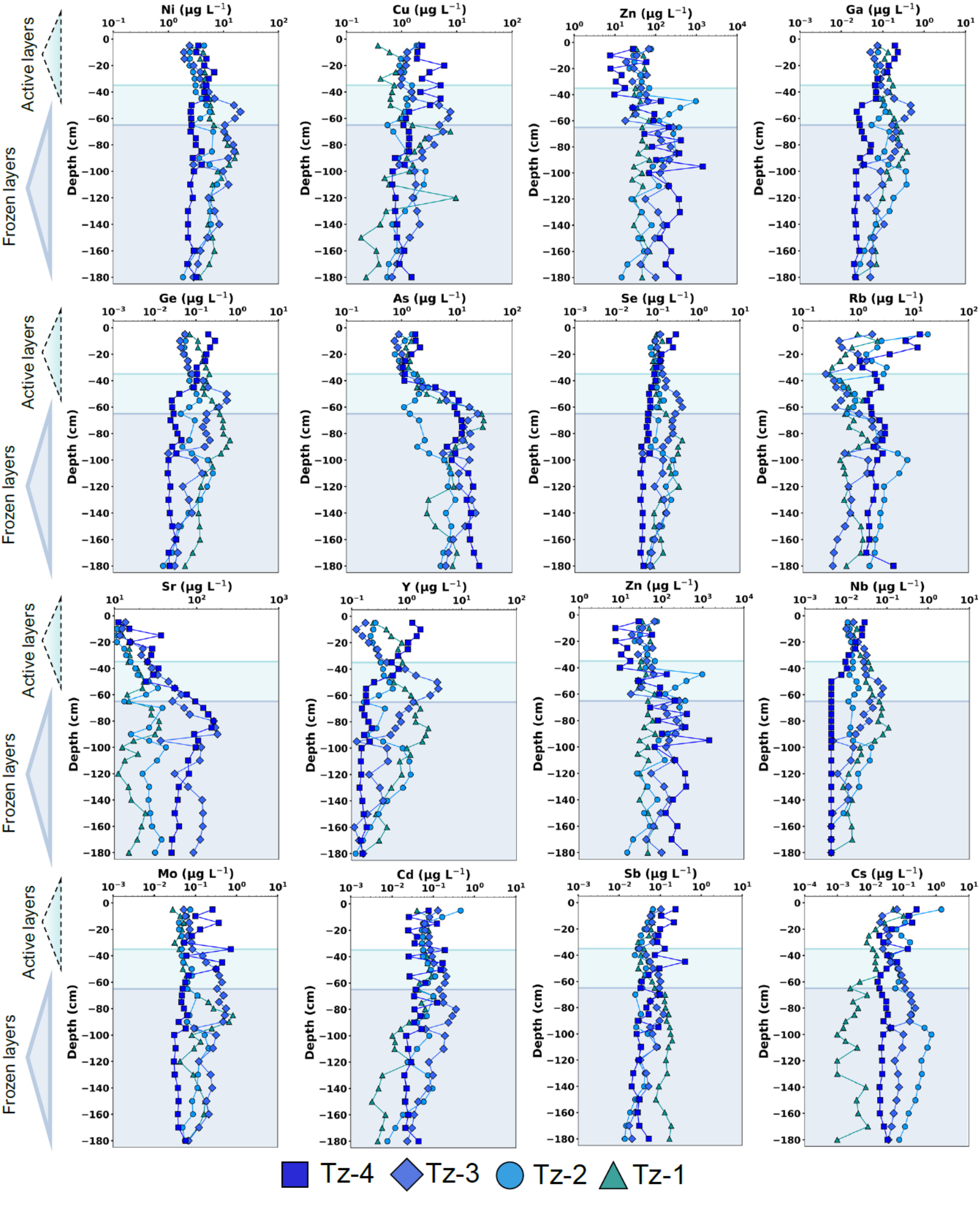

(continuation Figure S7)

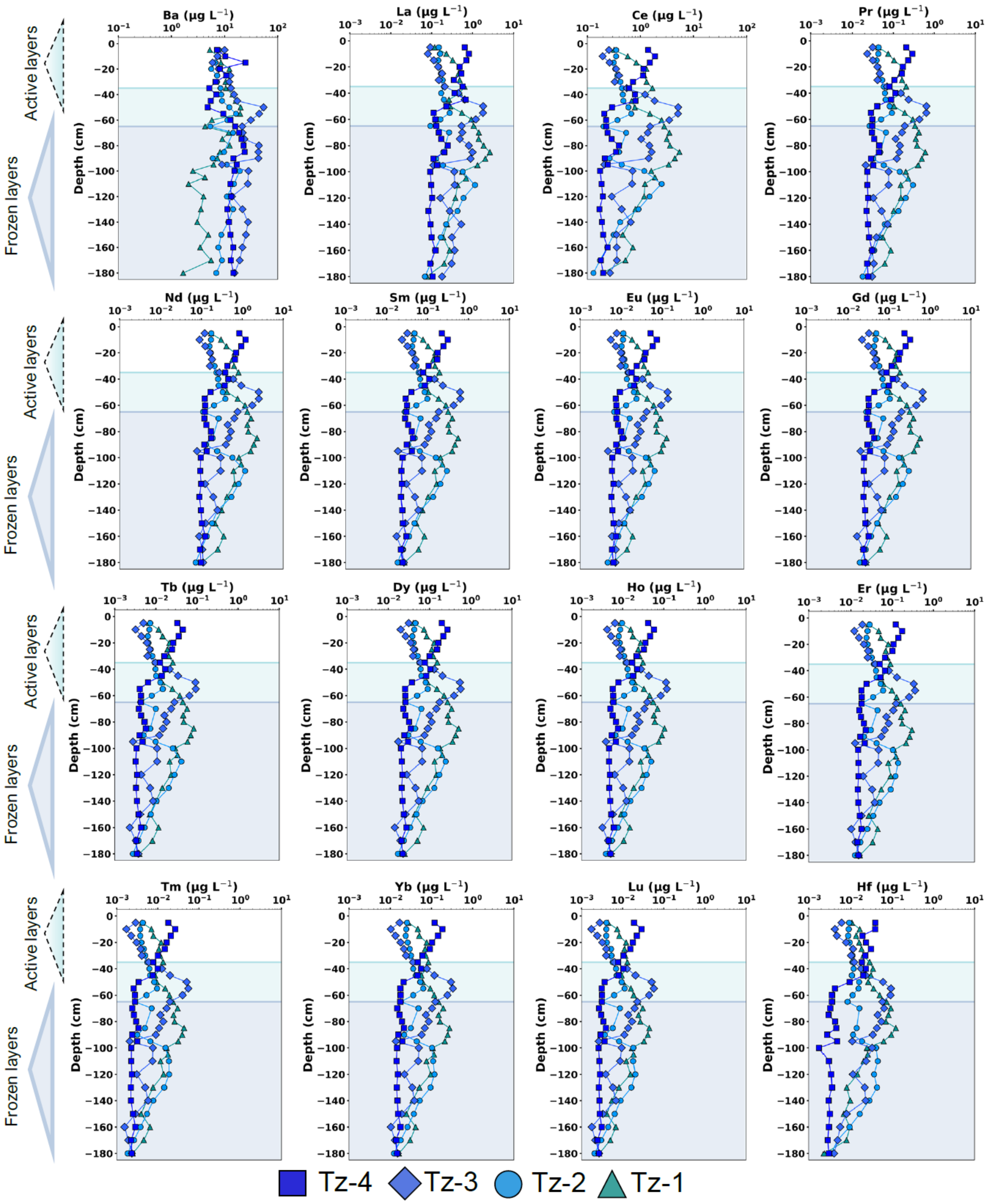

(continuation Figure S7)

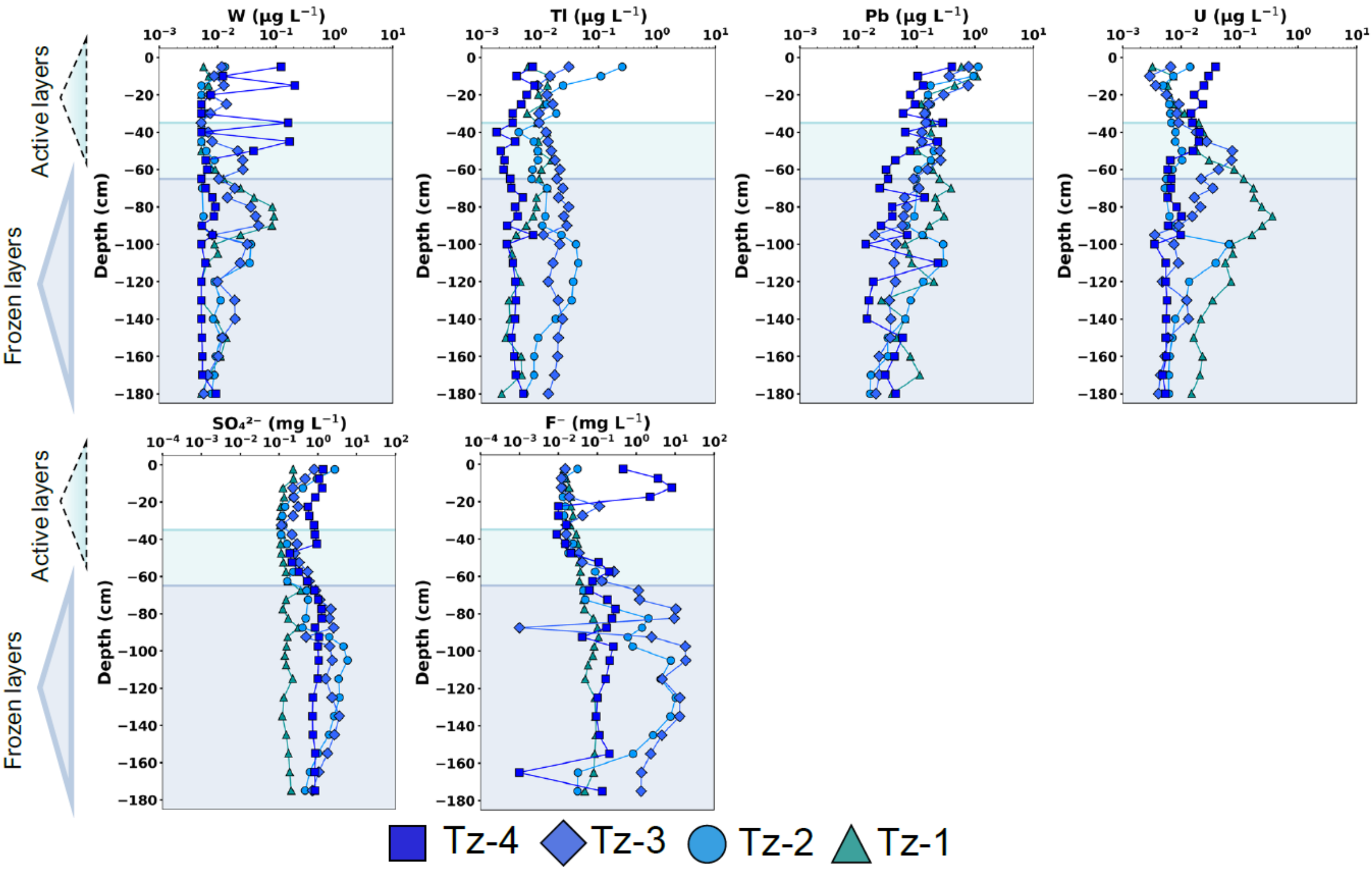

Figure S7. Concentration of majors, trace elements and anions (SO_4^{2-}, F^-) in the dissolved phase (< 0.45 µm) for porewater at the active layers and pore ice at the frozen layers for Tz-4, Tz-3, Tz-2 and Tz-1. The active layers (white and clear blue) thickness comprises the active layers depth measured at the moment of sampling (40 cm for Tz-4, 60 cm for Tz-3, 40 cm for Tz-2 and 55 cm for Tz-1). Permanent frozen layers (dark blue) are situated between 65 and 180 cm depth.

Note on the calculation of the Normalized Enrichment Factor (NEF)

The Normalized Enrichment Factor (NEF) is calculated as (Frozen - Active) / (Frozen + Active), where Frozen and Active represent the median concentrations in frozen and active layer samples for a given element, respectively for each sampling site (Tz-1 (AL, n = 11), (FL, n = 18); Tz-2 (AL, n = 8), (FL, n = 20); Tz-3 (AL, n = 12), (FL, n = 16); and Tz-4 (AL, n = 8), (FL, n = 20)).

Negative NEF values highlight the enrichment in the active layer porewaters, whereas positive NEF show the enrichment in pore ice at the frozen layer. Uncertainties were calculated using standard error propagation methods. Tests Mann-Whitney (MW) and t-test p-values (*** $p < 0.001$, ** $p < 0.01$, * $p < 0.05$, ns not significant) were used depending on the data normality and equal variance.

Table S5. Normalized enrichment factor (NEF)

	Tz-4					Tz-3				
Element	**NEF**	**SE**	**p-value**	**Significance**	**Test**	**NEF**	**SE**	**p-value**	**Significance**	**Test**
Li	0.45	0.14	0.0032	**	MW	0.62	0.06	1.42e-05	***	MW
Be	-0.72	0.04	1.29e-06	***	MW	0.20	0.24	0.9076	ns	MW
B	-0.08	0.14	0.1358	ns	MW	0.47	0.09	6.43e-04	***	MW
Na	-0.09	0.26	0.8617	ns	MW	0.02	0.12	0.8709	ns	MW
Mg	0.87	0.06	1.29e-06	***	MW	0.36	0.10	9.02e-04	***	MW
Al	-0.84	0.02	6.43e-07	***	MW	-0.05	0.20	0.2186	ns	MW
Si	-0.11	0.16	0.6005	ns	MW	-0.10	0.07	0.0115	*	t-test
K	-0.46	0.20	0.0213	*	MW	0.12	0.15	0.4718	ns	MW
Ca	0.53	0.11	7.72e-06	***	MW	0.73	0.07	2.16e-05	***	MW
Ti	-0.86	0.06	6.43e-07	***	MW	-0.67	0.12	1.28e-04	***	MW
V	-0.68	0.03	6.43e-07	***	MW	0.17	0.20	0.8345	ns	MW
Cr	-0.74	0.02	4.50e-06	***	MW	-0.29	0.12	0.0066	**	MW
Mn	0.85	0.12	1.29e-06	***	MW	0.72	0.11	7.21e-05	***	MW
Fe	-0.62	0.04	2.57e-06	***	MW	0.24	0.17	0.1436	ns	MW
Co	-0.19	0.07	0.0150	*	t-test	0.45	0.12	0.0028	**	MW
Ni	-0.27	0.05	1.21e-04	***	MW	0.38	0.19	0.2365	ns	MW
Cu	-0.35	0.10	1.66e-04	***	MW	0.15	0.15	0.7277	ns	MW
Zn	0.87	0.07	4.50e-06	***	MW	0.60	0.10	8.75e-05	***	MW
Ga	-0.67	0.09	1.29e-06	***	MW	-0.03	0.20	0.2753	ns	MW
Ge	-0.73	0.06	6.43e-07	***	MW	0.10	0.28	0.3653	ns	MW
As	0.80	0.04	6.43e-07	***	MW	0.86	0.09	1.28e-04	***	MW
Se	-0.41	0.11	6.43e-07	***	MW	0.04	0.12	0.5934	ns	MW
Rb	-0.22	0.25	0.2806	ns	MW	0.29	0.18	0.0739	ns	MW
Sr	0.49	0.10	2.90e-05	***	MW	0.65	0.08	3.98e-05	***	MW
Y	-0.72	0.06	1.29e-06	***	MW	0.04	0.32	0.5009	ns	MW
Zr	-0.78	0.03	2.57e-06	***	MW	0.37	0.24	0.5934	ns	MW
Nb	-0.59	0.08	2.40e-06	***	MW	-0.39	0.16	0.0190	*	MW
Mo	-0.43	0.17	0.0014	**	MW	0.52	0.17	0.0191	*	MW
Cd	-0.05	0.21	0.3542	ns	MW	0.14	0.19	0.9445	ns	MW
Sb	-0.50	0.11	6.60e-04	***	MW	-0.07	0.12	0.5214	ns	t-test
Cs	-0.59	0.24	0.0183	*	MW	0.40	0.14	0.0043	**	MW
Ba	0.29	0.08	0.0213	*	MW	0.28	0.11	0.0540	ns	MW
La	-0.65	0.05	1.93e-05	***	MW	0.31	0.27	0.4437	ns	MW
Ce	-0.67	0.06	4.50e-06	***	MW	0.18	0.33	1.0000	ns	MW
Pr	-0.70	0.06	1.29e-06	***	MW	0.12	0.32	0.5308	ns	MW
Nd	-0.70	0.06	6.43e-07	***	MW	0.09	0.32	0.3904	ns	MW
Sm	-0.71	0.07	1.29e-06	***	MW	0.05	0.30	0.2962	ns	MW
Eu	-0.67	0.08	1.29e-06	***	MW	0.14	0.31	0.4718	ns	MW
Gd	-0.71	0.06	1.29e-06	***	MW	0.09	0.32	0.3413	ns	MW
Tb	-0.73	0.06	1.29e-06	***	MW	0.07	0.30	0.3182	ns	MW
Dy	-0.73	0.06	1.29e-06	***	MW	0.09	0.31	0.3182	ns	MW
Ho	-0.72	0.05	1.29e-06	***	MW	0.11	0.33	0.3653	ns	MW
Er	-0.72	0.06	1.29e-06	***	MW	0.13	0.33	0.4166	ns	MW
Tm	-0.72	0.06	6.43e-07	***	MW	0.13	0.32	0.5009	ns	MW
Yb	-0.71	0.07	6.43e-07	***	MW	0.18	0.34	0.7277	ns	MW
Lu	-0.70	0.06	1.29e-06	***	MW	0.20	0.33	0.7628	ns	MW
Hf	-0.76	0.03	2.57e-06	***	MW	0.33	0.25	0.6259	ns	MW
W	-0.24	0.37	0.3431	ns	MW	0.25	0.16	0.1858	ns	MW
Tl	-0.09	0.11	0.1816	ns	MW	0.18	0.06	0.0168	*	MW
Pb	-0.45	0.12	0.0021	**	MW	-0.66	0.09	9.27e-06	***	MW
U	-0.58	0.06	1.22e-05	***	MW	0.00	0.26	0.4718	ns	MW
DOC	0.26	0.06	0.0081	**	MW	0.40	0.07	1.54e-04	***	MW
TDN	0.65	0.13	0.0011	**	MW	0.88	0.05	1.57e-05	***	MW
TDP	0.68	0.27	0.0487	*	MW	0.88	0.06	2.16e-05	***	MW

	Tz-2					Tz-1				
Element	**NEF**	**SE**	**p-value**	**Significance**	**Test**	**NEF**	**SE**	**p-value**	**Significance**	**Test**
Li	0.26	0.06	0.0014	**	MW	0.34	0.09	6.96e-05	***	MW
Be	0.22	0.07	0.0625	ns	MW	-0.34	0.18	0.1704	ns	MW
B	0.19	0.08	0.0023	**	MW	0.46	0.06	9.31e-06	***	MW
Na	0.22	0.14	0.4385	ns	MW	0.69	0.05	3.22e-05	***	MW
Mg	0.20	0.11	0.1991	ns	MW	0.43	0.08	6.96e-05	***	MW
Al	0.17	0.11	0.1226	ns	MW	-0.77	0.13	4.18e-04	***	MW
Si	0.13	0.07	0.0428	*	MW	-0.24	0.20	0.2336	ns	MW
K	0.23	0.21	0.4092	ns	MW	0.45	0.11	3.53e-04	***	MW
Ca	0.31	0.07	2.98e-04	***	MW	0.28	0.08	9.55e-04	***	MW
Ti	-0.18	0.09	0.0887	ns	MW	-0.32	0.20	0.1210	ns	MW
V	0.15	0.10	0.2177	ns	MW	-0.29	0.15	0.1210	ns	MW
Cr	-0.07	0.09	0.6005	ns	MW	0.06	0.14	0.7702	ns	MW
Mn	0.45	0.09	1.29e-06	***	MW	0.74	0.07	9.54e-06	***	MW
Fe	0.12	0.10	0.1991	ns	MW	0.13	0.19	0.4583	ns	MW
Co	0.17	0.09	0.1816	ns	MW	0.09	0.08	0.0919	ns	MW
Ni	0.28	0.07	0.0157	*	MW	0.19	0.08	4.95e-04	***	MW
Cu	-0.14	0.09	0.0991	ns	MW	0.23	0.20	0.4860	ns	MW
Zn	0.49	0.16	0.0183	*	MW	0.05	0.07	0.2048	ns	t-test
Ga	0.13	0.11	0.2584	ns	MW	0.00	0.16	0.8750	ns	MW
Ge	0.14	0.10	0.2177	ns	MW	0.19	0.17	0.1441	ns	MW
As	0.60	0.14	1.66e-04	***	MW	0.70	0.06	1.77e-05	***	MW
Se	0.05	0.08	0.3285	ns	MW	0.38	0.09	0.0018	**	MW
Rb	-0.08	0.15	0.8227	ns	MW	0.01	0.11	0.4583	ns	MW
Sr	0.33	0.05	1.22e-05	***	MW	0.08	0.09	0.2164	ns	MW
Y	0.17	0.09	0.2177	ns	MW	0.22	0.16	0.1106	ns	MW
Zr	0.21	0.08	0.0285	*	MW	0.23	0.23	0.2909	ns	MW
Nb	0.03	0.07	0.4606	ns	MW	0.01	0.24	0.6694	ns	MW
Mo	0.29	0.07	1.66e-04	***	MW	0.43	0.08	5.75e-05	***	MW
Cd	0.11	0.16	1.0000	ns	MW	-0.67	0.16	3.53e-04	***	MW
Sb	-0.06	0.11	0.4688	ns	MW	0.54	0.08	1.17e-05	***	MW
Cs	0.16	0.17	0.2584	ns	MW	-0.65	0.09	1.44e-05	***	MW
Ba	0.20	0.06	0.0032	**	MW	-0.41	0.09	8.37e-05	***	t-test
La	0.08	0.09	0.2806	ns	MW	0.16	0.22	0.1849	ns	MW
Ce	0.13	0.10	0.3039	ns	MW	0.19	0.20	0.1568	ns	MW
Pr	0.17	0.09	0.1653	ns	MW	0.19	0.19	0.1704	ns	MW
Nd	0.18	0.09	0.1653	ns	MW	0.21	0.18	0.1106	ns	MW
Sm	0.16	0.09	0.1816	ns	MW	0.22	0.16	0.1210	ns	MW
Eu	0.15	0.08	0.1358	ns	MW	0.21	0.17	0.1321	ns	MW
Gd	0.18	0.08	0.1226	ns	MW	0.23	0.16	0.1009	ns	MW
Tb	0.15	0.08	0.1500	ns	MW	0.25	0.16	0.1009	ns	MW
Dy	0.17	0.08	0.1358	ns	MW	0.26	0.15	0.1009	ns	MW
Ho	0.18	0.09	0.1103	ns	MW	0.25	0.16	0.1106	ns	MW
Er	0.20	0.09	0.0887	ns	MW	0.25	0.15	0.1106	ns	MW
Tm	0.21	0.09	0.0792	ns	MW	0.23	0.16	0.1441	ns	MW
Yb	0.24	0.09	0.0428	*	MW	0.23	0.15	0.1106	ns	MW
Lu	0.28	0.09	0.0375	*	MW	0.23	0.13	0.1210	ns	MW
Hf	0.23	0.08	0.0247	*	MW	0.11	0.28	0.7024	ns	MW
W	0.21	0.11	0.0895	ns	MW	0.34	0.11	9.40e-04	***	MW
Tl	-0.17	0.23	0.3542	ns	MW	-0.33	0.11	0.0011	**	MW
Pb	-0.24	0.18	0.0375	*	MW	-0.18	0.18	0.1210	ns	MW
U	0.06	0.08	0.3542	ns	MW	0.74	0.14	2.09e-04	***	MW
DOC	0.46	0.08	6.43e-07	***	MW	-0.07	0.10	0.7024	ns	MW
TDN	0.81	0.05	6.43e-07	***	MW	0.16	0.11	0.0024	**	MW
TDP	0.67	0.18	0.0026	**	MW	-0.11	0.17	0.7702	ns	MW

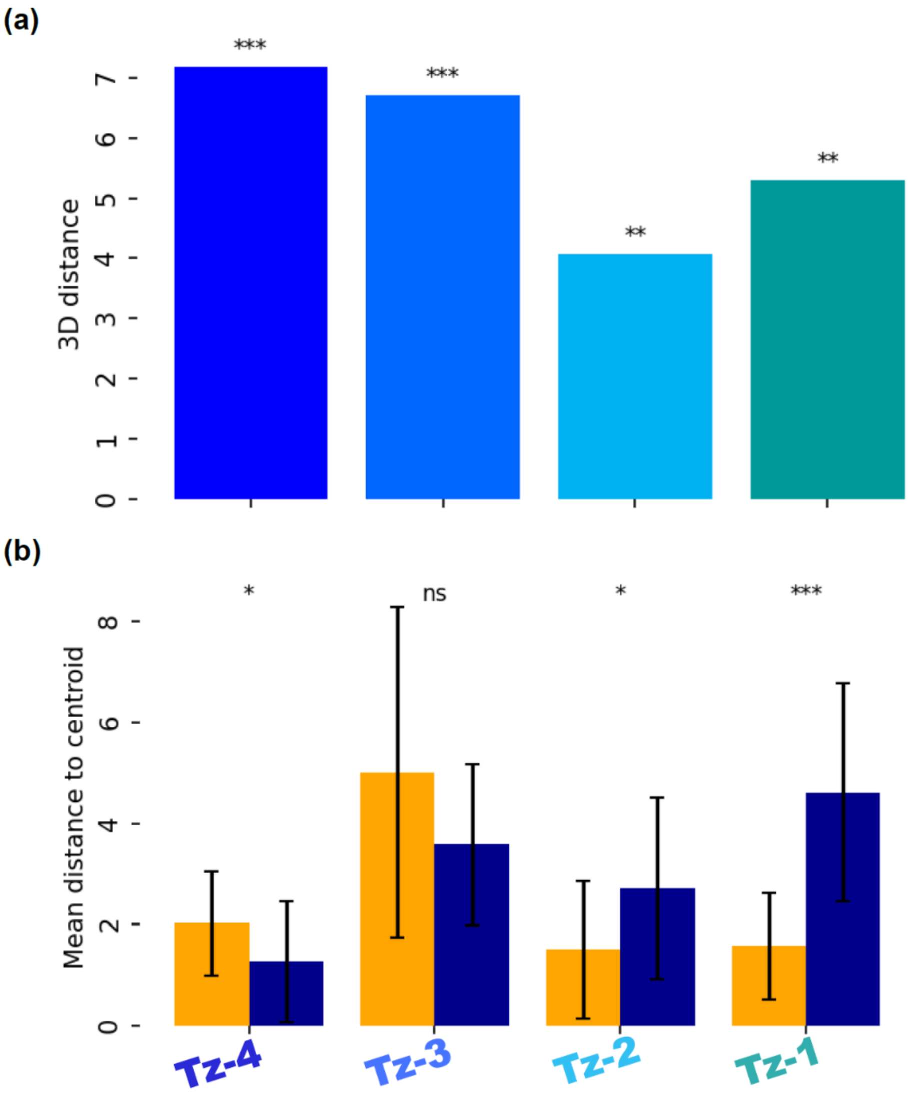

Figure S8. (a) Three-dimensional Euclidean distance between active and frozen centroids calculated separately for each site and (b) within-site dispersion of samples for each compartment (active layer, in orange, and frozen layer, in blue), expressed as the mean distance to the corresponding site centroid (*** p < 0.001, ** p < 0.01, * p < 0.05, ns = not significant). Samples correspond to the dissolve fraction (< 0.45 µm) for porewater at the active layers and pore ice at the frozen layers for Tz-4, Tz-3, Tz-2 and Tz-1.

Within individual soil columns (Fig. S8a), the 3D centroid distance between active and frozen compartments is greatest at Tz-4, followed by Tz-3, Tz-1 and Tz-2, indicating variable magnitude of compartmental contrast among microsites, suggesting a greater homogenization at lower positions at the thaw sequence (bog Tz-4 ⟶ trough Tz-3 ⟶ transitional fen Tz-2 ⟶ peat-mineral fen Tz-1).

Regarding dispersion within each site (Fig. S8b), Tz-4 frozen samples are closer to their site centroid and significantly different from the corresponding active layer ($p < 0.05$). For Tz-3 (p = ns), the influence of the microsite is not significant on the composition of the active and frozen samples. At Tz-2 ($p < 0.05$), frozen layer samples are closer to the corresponding site centroid, as it is the case for Tz-1 ($p < 0.001$), where the mineral nature of the frozen layer plays a highly significant role in frozen layer composition.

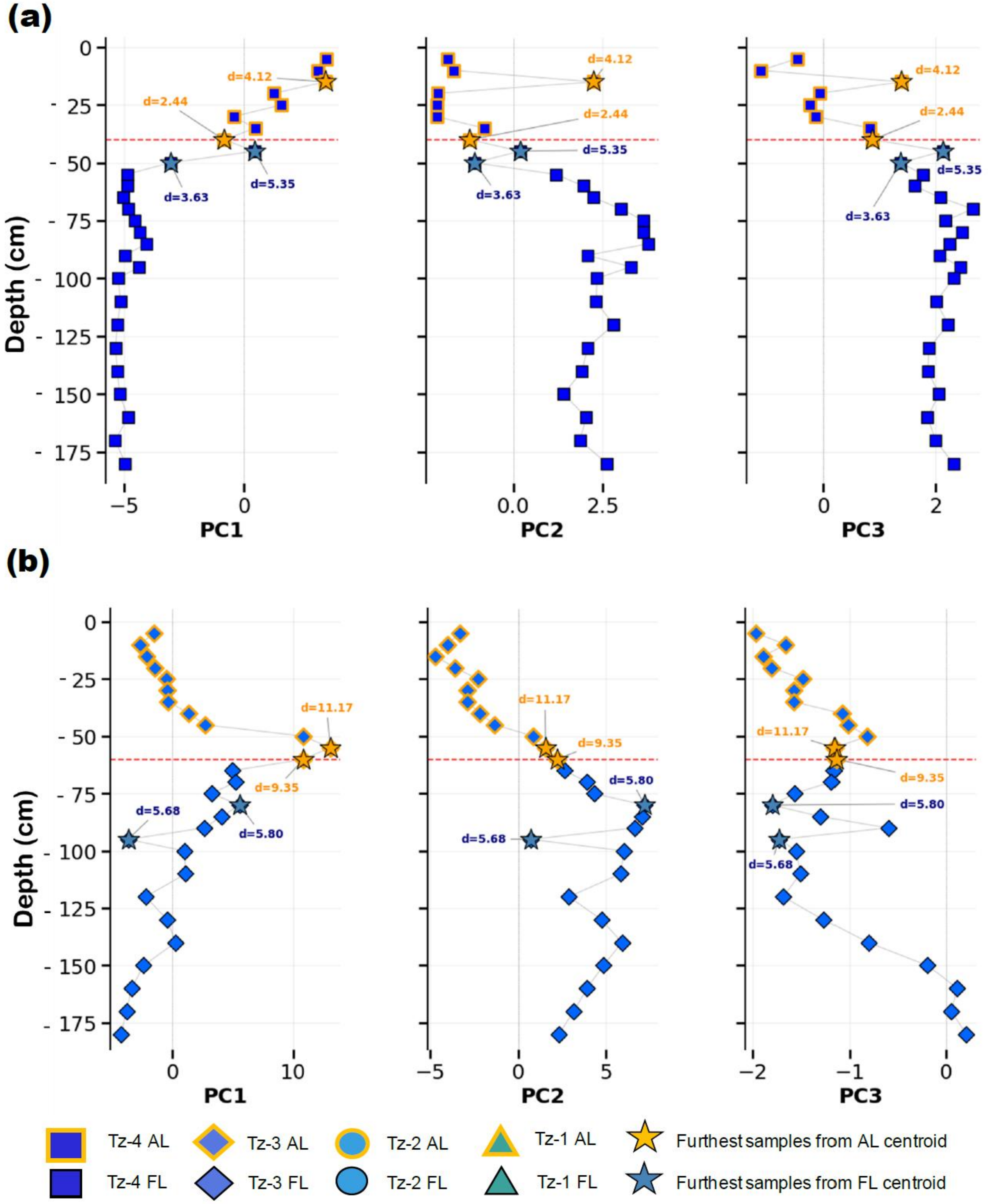

(a)
(b)
Depth (cm)
PC1
PC2
PC3
d=4.12
d=2.44
d=5.35
d=3.63
d=11.17
d=9.35
d=5.80
d=5.68
Tz-4 AL
Tz-4 FL
Tz-3 AL
Tz-3 FL
Tz-2 AL
Tz-2 FL
Tz-1 AL
Tz-1 FL
Furthest samples from AL centroid
Furthest samples from FL centroid

(continuation Figure S9)

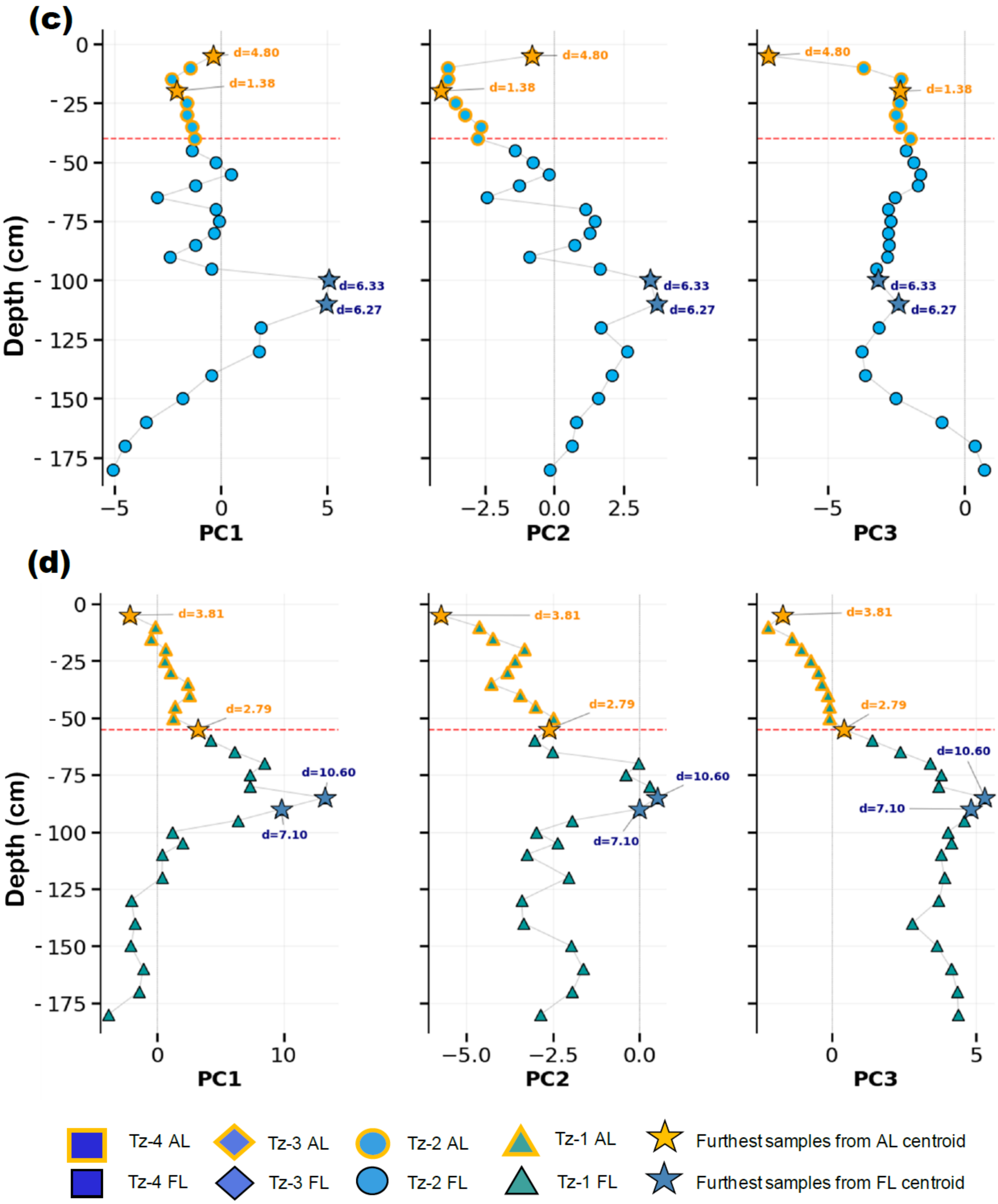

Figure S9. PCA scores (PC1, PC2 and PC3) vs depth profiles. Dotted red line represents the active layer thickness at the time of sampling. Distances (d) represent the PCA units away from the average position of active layer (AL) samples and frozen layer (FL) samples at each corresponding site **(a)** Tz-4, **(b)** Tz-3, **(c)** Tz-2 and **(d)** Tz-1.

At Tz-4, frozen samples show minimal variation along PC1 and PC3, although samples at 15 cm and 40–45 cm (active layer limit) deviate from their respective group centroids (Fig. S9a). At Tz-3, the most distant active layer sample is driven by PC1, whereas the frozen-layer peak (80–95 cm) is controlled by PC2 (Fig. S9b). For Tz-2, the main peak between 95 and 130 cm depth—particularly at 100 and 110 cm—is influenced by both PC1 and PC2 (Fig. S9c), while shallow active layer samples (5 and 20 cm) are furthest from the active centroid. At Tz-3, a deeper anomaly at 180 cm appears to be associated with PC3. At Tz-1, frozen-layer peaks between 80 and 100 cm are significantly driven by PC1, followed by PC2 (Fig. S9d). The active layer depth at sampling and the surface horizon (0–5 cm) at Tz-1 also deviate from the active centroid. Notably, Tz-1 pore ice below 125 cm displays negative PC1 values similar to deeper frozen samples at Tz-4, Tz-3 and below 140 cm at Tz-2.

.

References cited

Beckwith, C. W., Baird, A. J., and Heathwaite, A. L.: Anisotropy and depth-related heterogeneity of hydraulic conductivity in a bog peat. I: laboratory measurements, Hydrological Processes, 17, 89–101, https://doi.org/10.1002/hyp.1116, 2003.

Byun, E., Rezanezhad, F., Slowinski, S., Lam, C., Bhusal, S., Wright, S., Quinton, W. L., Webster, K. L., and Van Cappellen, P.: Effects of nitrogen and phosphorus amendments on CO2 and CH4 production in peat soils of Scotty Creek, Northwest Territories: potential considerations for wildfire and permafrost thaw impacts on peatland carbon exchanges, SOIL, 11, 309–321, https://doi.org/10.5194/soil-11-309-2025, 2025.

Drake, T. W., Wickland, K. P., Spencer, R. G. M., McKnight, D. M., and Striegl, R. G.: Ancient low–molecular-weight organic acids in permafrost fuel rapid carbon dioxide production upon thaw, Proc. Natl. Acad. Sci. U.S.A., 112, 13946–13951, https://doi.org/10.1073/pnas.1511705112, 2015.

Estop-Aragonés, C., Heffernan, L., Knorr, K.-H., and Olefeldt, D.: Limited Potential for Mineralization of Permafrost Peatland Soil Carbon Following Thermokarst: Evidence From Anoxic Incubation and Priming Experiments, Journal of Geophysical Research: Biogeosciences, 127, e2022JG006910, https://doi.org/10.1029/2022JG006910, 2022.